

Interfacial dynamics and frequencies of passive bubble-acoustic emissions

Richard Manasseh (1,2,3) Anh Bui (3) Petar Liovic (3) Andrew Ooi (2)

Guillaume Riboux (4) and Frédéric Risso (5)

(1) Faculty of Engineering & Industrial Sciences,

Swinburne University of Technology, Hawthorn, VIC 3122, Melbourne, Australia

(2) Department of Mechanical Engineering, University of Melbourne, VIC 3010, Melbourne, Australia

(3) Fluid Dynamics, CSIRO, Highett VIC 3190, Melbourne, Australia

(4) Escuela Superior de Ingenieros, Universidad de Sevilla, Spain

(5) Institut de Mécanique des Fluides de Toulouse, UMR 5502 CNRS-INP-UPS, Université de Toulouse, France

PACS: 43.25.Ts, 47.35.Rs, 47.55.D-, 47.55.dd, 47.55.dr, 47.55.dp

ABSTRACT

The status of numerical predictions of the natural emission of sound by bubbles is reviewed. High-amplitude sound is generally emitted during events such as bubble pinch-off from an orifice, fragmentation, or coalescence: cases when there are brief, extreme distortions to the gas-liquid interface. While well-established theory relates bubble sizes to their natural emission frequencies, practical measurements are complicated by uncertainly on the sound amplitude emitted by individual bubbles, which is determined by the fluid dynamics of the event. Benchmark experimental data was previously generated by the coalescence of bubbles; such events inherently involve extreme distortions to the interface. Numerical calculations by a two-dimensional axisymmetric compressible level-set code are presented, simulating the experimental conditions. This method gives good predictions of the interfacial kinematics and oscillation frequency but less realistic predictions of the acoustic amplitude. A second approach employs a three-dimensional multi-material code, and is significantly more computationally intensive. Preliminary results on a spherically perturbed bubble show that an excellent agreement with the oscillation frequency can be obtained, in cases where the bubble is both far from and close to a wall.

INTRODUCTION

In physical terms, a gas bubble is a compressible ‘spring’ connected to the surrounding mass of liquid and hence, like any mass-spring system, the gas volume can oscillate with a natural frequency. A combination of the equations of mass and momentum conservation for a liquid of infinite extent surrounding a spherically-symmetric, volumetrically-oscillating gas bubble leads to the Rayleigh-Plesset equation (Rayleigh 1917, Plesset and Prosperetti 1977),

$$R \frac{d^2 R}{dt^2} + \frac{3}{2} \left(\frac{dR}{dt} \right)^2 = \frac{1}{\rho} \left(P_g - p_\infty - \frac{2\sigma}{R} - 4 \frac{\mu}{R} \frac{dR}{dt} \right), \quad (1)$$

where R is the instantaneous bubble radius, P_g is the pressure in the bubble, p_∞ is the liquid pressure far from the bubble, σ is the surface tension, and μ is the dynamic viscosity. Linearisation of (1) for small-amplitude, inviscid oscillations, neglecting surface tension, and using the ideal gas law to relate the bubble radius to P_g , gives a simple harmonic equation. The resulting natural frequency was first predicted by Minnaert (1933) for millimetre-sized bubbles. Minnaert’s equation (1933) gives the natural frequency f_0 as,

$$f_0 = \frac{1}{2\pi} \sqrt{\frac{3\gamma P_0}{\rho}} \cdot \frac{1}{R_0}, \quad (2)$$

where γ is the ratio of specific heats of gas inside the bubble, P_0 is the absolute liquid pressure which equals p_∞ when surface tension is neglected, ρ is the liquid density and R_0 is the equilibrium bubble radius.

Repeated experiments have demonstrated that (2) is appropriate for the assumptions under which it was derived (Strasberg 1953, Longuet-Higgins et al. 1991, Manasseh et al. 2004). Even in complex systems of bubbles, frequencies based on the assumptions behind (1) compare reasonably well with experiment (Manasseh and Ooi 2009). However, the mechanism or mechanisms with which bubble sound emissions are initiated remain unclear. Thus, unlike the frequency, the amplitude of bubble sound emissions is difficult to predict.

Passive emission of small-amplitude sound by bubbles is common in many practical industrial flows (Hsi et al. 1985, Boyd and Varley 2001, Manasseh et al. 2001b) or environmental flows (Melville et al. 1988, Ding and Farmer 1994, Manasseh et al. 2006). The difficulty in predicting the amplitude is one problem in the interpretation of the signals from such sources (Boyd and Varley 2001, Manasseh et al. 2001b), leading to complex signal-processing approaches (Al-Masry et al. 2005, Manasseh et al. 2006). Numerical simulations of compressible multiphase flows have advanced in quality (e.g. Oğuz and Prosperetti 1993, Prosperetti and Oğuz 1993, Hu and Khoo 2004, Manasseh et al. 2001a, Bui and Manasseh 2006, Klaseboer and Khoo 2004). However, careful comparison with matching laboratory experiments is required. A particular issue is control over the interfacial curvature in compressible multiphase flow (e.g. Liovic et al. 2009).

Longuet-Higgins (Longuet-Higgins 1990) proposed three general mechanisms by which the energy giving an initial acoustic

perturbation could be imparted to the bubble: (i) a difference in instantaneous Laplace pressure at the instant the bubble is formed; (ii) the radial inrush of liquid as the pinch-off occurs; and (iii) an excitation (Longuet-Higgins 1989) by nonlinear interactions of shape modes of the volumetric or ‘breathing’ mode of the bubble. It is likely that some of these mechanisms might apply in some situations, but not in others (Leighton 1994).

Bubbles can emit sound on pinch-off from a parent body of gas. This event could lead to mechanism (ii). It was first observed by Knud Lunde (see Leighton 1994) that a high-speed liquid jet penetrates the bubble on the breaking of the neck that joins it to its parent body of gas, and may be responsible for compressing the trapped gas (Manasseh et al. 1998). Recently, Deane and Czerski (2008) obtained excellent experimental imaging of the jet and used the experimental interfacial kinematics to calculate a forcing function for the Rayleigh-Plesset equation. Longuet-Higgins (Longuet-Higgins et al. 1991) also proposed that orifice-formed bubbles could make sound by mechanism (iii).

Bubbles are often formed from a free surface. This is common in situations such as raindrop impact (e.g. Pumphrey and Elmore 1990, Pumphrey and Crum 1990), plunging jets (e.g. Hahn et al. 2003, Chanson and Manasseh 2003) and wave-breaking (e.g. Melville et al. 1988, Loewen and Melville 1991, Ding and Farmer 1994, Manasseh et al. 2006). Once the surface closes, forming the bubble, there must be a sudden transition from a cavity at atmospheric pressure to a closed bubble in which the pressure exceeds atmospheric by the Laplace pressure due to surface tension, plus the hydrostatic pressure that must now be supported. Thus, in this second class of phenomena, mechanism (i) is a possible explanation as well as (ii) and (iii). Pumphrey & Elmore (Pumphrey and Elmore 1990) created bubbles from drop impacts in the laboratory. However, the amplitude predicted by Laplace-pressure theory was only about 25% of the experimental values, and the trend with bubble size was not predicted. One issue in most laboratory-tank experiments is the presence of reverberation from the tank walls, which in some cases could alter the measured frequency as well as amplitude.

Manasseh et al. (2008) also proposed a Laplace-pressure equalisation theory; their experiment on coalescing bubbles and results are outlined below. The present paper reviews compressible multiphase numerical simulations of these experiments. The present paper also presents more fundamental high-resolution three-dimensional calculations that may ultimately be necessary to predict the amplitude.

EXPERIMENTS

Experimental Method

The experiments used to benchmark numerical calculations were detailed by Manasseh et al. (2008), so only brief details are reproduced here. The test section was a glass tank 1,000 mm high with a square cross-section of 150 mm. The tank was filled with filtered tap water at a temperature between 16 and 17°C. Air bubbles of 1.6 mm diameter were injected at 85 mm from the bottom of the tank by a needle with an internal diameter of 0.1 mm and a length of 100 mm. The rate of bubble production was controlled by adjusting the pressure in the tank to which the needle is connected.

A high-speed digital video camera (Photron Ultima APX) was used to film the bubble detachment from the tip of the needle at a frame rate of 20,000 Hz and with an exposure time of 1/87,600 s. The region imaged was 1.113 mm high and 2.226 mm wide with a resolution 128 × 256 pixels. Images of the

bubbles were processed to extract their equivalent spherical radius and location as a function of time (Ellingsen and Risso 2001).

In Manasseh et al. (2008), a Brüel & Kjaer type 8103 hydrophone pre-amplified by a Brüel & Kjaer type 2635 charge amplifier was used to transduce the acoustic signal. Distances were calculated from the true acoustic centre of the 9.5 mm diameter hydrophone and Manasseh et al. (2008) detailed the signal conditioning and processing procedures; the signal was logged at 120 kHz. The distance from the acoustic centre to the bubble centre was 19.1 ± 0.1 mm. Owing to the concerns about reverberations in small tanks, Manasseh et al. (2008) reported tests confirming that the sound field fell off approximately as $1/r$, where r is the distance from the bubble centre, rather than being significantly affected by sound wave modes or reverberations. The acoustic and video data were precisely co-registered by a careful procedure accounting for minor shifts in digital electronic acquisition rates.

Acoustic time series and photo-montages of the high-speed video frames were generated over the same time window so that acoustic and visual events could be clearly correlated. Since most of the interesting variations occur on the centreline of the bubble image, a montage of a strip of pixels bracketing the centreline of the image preserved much of the relevant information content (Manasseh et al. 2008). In the extreme, a montage of strips each only 1 pixel wide would be a ‘time-space diagram’ (e.g. Goharzadeh and Mutabazi 2001) showing the rate at which events move along the centreline.

NUMERICAL METHODS

Axisymmetric level-set method

A compressible, multiphase simulation of the experiments of (Manasseh et al. 2008) was implemented by an axisymmetric level-set model. The calculation was based on the level-set method to track the interfaces, and an explicit flow solver for compressible and nearly incompressible multiphase flows. The gas and liquid are treated as a single continuum fluid with properties varying continuously from gas to liquid states. Coupled with a high-resolution advection scheme, this modelling approach allows the description of the movement of gas and fluid and the deformation of the interface separating them on a fixed computational mesh (Bui and Manasseh 2006).

Using a single-field formalism for describing a gas-liquid flow featuring well-resolved interfaces, the momentum equation is

$$\frac{\partial \rho \mathbf{U}}{\partial t} + \nabla \cdot (\rho \mathbf{U} \mathbf{U}) = -\nabla P + \rho \mathbf{g} + \nabla \cdot \boldsymbol{\tau} + \sigma \kappa \hat{\mathbf{n}}_i \delta, \quad (3)$$

where $\boldsymbol{\tau}$ is the stress tensor, $\sigma \kappa \hat{\mathbf{n}}_i \delta$ is the surface tension force that is non-zero only at the interface, σ is the surface tension coefficient, and $\hat{\mathbf{n}}$ is the interface orientation.

The compressible-nearly incompressible flow solver was furthermore based on the solution of an additional differential equation for pressure which was derived from the laws of mass and energy conservation,

$$\frac{\partial p}{\partial t} + \mathbf{U} \cdot \nabla p = -\rho c^2 \nabla \cdot \mathbf{U}, \quad (4)$$

where c is the sound speed defined as

$$c^2 = \gamma \left(\frac{p + p_\infty}{\rho} \right),$$

where p_∞ is a stiffness parameter which is zero for the gas.

A generic equation of state of the form

$$\rho e = \frac{p + \gamma p_\infty}{\gamma - 1}, \quad (5)$$

was used, where e is the internal energy. As in the presentation of the Rayleigh-Plesset equation and solution (1)-(2), the parameter γ has the usual meaning of the ratio of specific heats for the gas, but is used in conjunction with p_∞ to define the compressibility of the liquid.

To track the evolution of the interface, a *level function* is advected by the flow. This function is chosen as a signed distance function with the zero level set defining the interface location Osher and Sethian (1988), and has the form

$$\phi_t + (\mathbf{U} \cdot \nabla) \phi = 0. \quad (6)$$

Using the level function, the steep changes of fluid properties across the interface were smoothed out to minimize numerical oscillations in the solution of Navier-Stokes equations. The level function was also used to calculate interfacial geometrical properties, such as the normal vector, \vec{n} , and the interfacial curvature, κ , as follows:

$$\vec{n} = \frac{\nabla \phi}{|\nabla \phi|}, \quad \kappa = \nabla \cdot \vec{n},$$

which in turn define the surface tension.

The system of differential equations describing the fluid and interface motions was solved using a predictor-corrector method (see Yoon and Yabe (1999)). The high-resolution numerical schemes ENO (Essentially-Non-Oscillatory) or WENO (Weighted ENO) was used for the convective flux calculation.

Three-dimensional Volume-of-Fluid method

A three-dimensional multi-material flow solution algorithm based on Volume-of-Fluid (VOF) Hirt and Nichols (1981) interface tracking was also considered as an alternative to the level-set method. Advantages associated with using the 3D VOF-based solution algorithm may include a greater control over interfacial curvature (Liovic et al. 2009), which may be relevant to modelling the extreme distortions to the surface of mechanism (ii). The provision of three-dimensionality allows the capturing of non-axisymmetric phenomena which may be inherent to mechanism (iii), with the disadvantage of a much greater computational cost. For the present paper, this code is to be validated against analytic theory for a spherically-perturbed, spherical bubble as a prelude to the sort of calculation presented for the axisymmetric level-set code.

The 3D VOF-based flow solver again involves generation of coupled gas-sided and liquid-sided flow fields, with coupling achieved through interface tracking and through enforcement of physics at interfaces between fluids in the form of jump conditions. This approach is chosen in preference to the combination of liquid-only flow simulators with vapor models, because of its versatility in being able to capture gas-sided flow patterns. In VOF methods, a phase indicator or *color function*

$$C(\mathbf{x}) = \begin{cases} 1 & \text{if } \mathbf{x} \text{ occupied by phase } k = G \\ 0 & \text{if } \mathbf{x} \text{ occupied by phase } k = L \end{cases} \quad (7)$$

is introduced to identify the location of the interface at any moment in simulated time, with the interface implicitly defined by the spatial distribution $C(x, y, z)$ in the discrete sense as regions of $0 < C < 1$. VOF methods use the color function for the purpose of interface tracking according to the advection equation

$$\frac{\partial C}{\partial t} + \mathbf{U} \cdot \nabla C = 0, \quad (8)$$

where $\mathbf{U}(x, y, z)$ is the velocity field. The C -weighted local density is defined as

$$\rho = C\rho_G + (1 - C)\rho_L. \quad (9)$$

The same thermodynamic relations as presented for the level-set flow solver also apply here.

The flow solver used to solve the small-scale flows described in this paper is the MFVOF-3D code Liovic et al. (2006), Liovic and Lakehal (2007b;a), Liovic et al. (2009). The flow solver is based on finite-difference methods applied to orthogonal meshes. For various terms in the governing equations, discretizations variously described as being finite-difference or finite-volume are used to promote consistency and conservation in simulated solutions. The MFVOF-3D code features 3D PLIC-VOF for interface tracking on a mesh twice as fine as the flow field mesh as proposed in Rudman (1998). The Centroid-Vertex Triangle-Normal Averaging (CVTNA) scheme for interface reconstruction Liovic et al. (2006) enables second-order accuracy in interface tracking to be achieved, and unsplit advection in 3D Liovic et al. (2006), Liovic and Lakehal (2008) enables this to be achieved in a single-stage VOF method while locally conserving mass. The array of advanced numerics included in the MFVOF-3D software is described in more detail in Liovic et al. (2006), Liovic and Lakehal (2007a), Liovic et al. (2009).

Experimental Results

As detailed by Manasseh et al. (2008), at very low bubble production rates f_b less than 3.5 s^{-1} , a series of single bubbles was formed, generating very low sound amplitudes. A threshold was found at $3.8 \pm 0.1 \text{ s}^{-1}$ above which a small, ‘secondary’ bubble formed and coalesced with the first bubble. This process generated sound amplitudes an order magnitude greater than the detachment process. These emissions were thus just like any individual bubble-acoustic pulse reported in the literature (e.g. Minnaert 1933, Strasberg 1956, Leighton and Walton 1987, Manasseh et al. 2001b). Loud sound emission under circumstances of bubble coalescence has been noted before (Leighton et al. 1991).

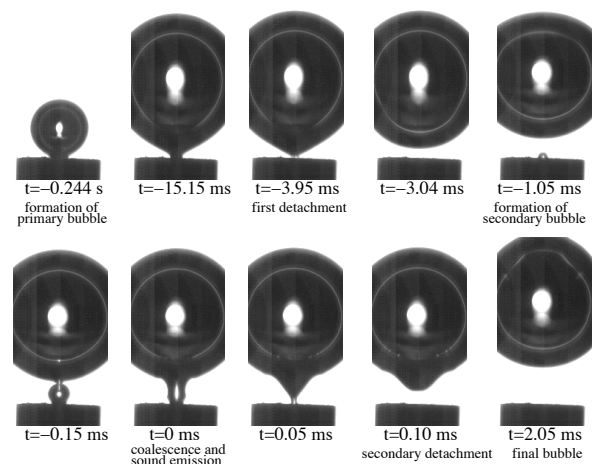


Figure 1: Bubble formation sequence. Bubble production rate f_b is 3.8 s^{-1} , bubble diameter 1.6 mm. From Manasseh et al. (2008).

The circumstances leading to in-line pairing and subsequent coalescence of orifice-formed bubbles have been studied before, particularly in the chemical engineering literature (Nevers and Wu 1971, Bhaga and Weber 1980, Stewart 1995, Manasseh 1996). However, most detailed coalescence studies are for the pairing and coalescence of equal-sized bubbles.

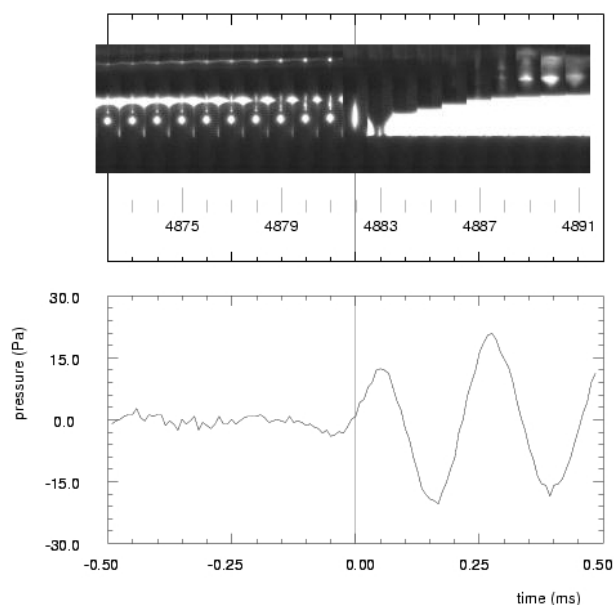


Figure 2: Time-series of video and acoustic data over a time of 1 ms. Bubble production rate f_b is 3.8 s^{-1} , bubble diameter 1.6 mm. Secondary scale in upper panel shows video frame numbers. From Manasseh et al. (2008).

As the air flow rate was increased, Manasseh et al. (2008) noticed further coalescences occurred with each primary bubble, with the number of coalescences increasing with air flow rate and each coalescence regime being quite repeatable. Like the binary in-line coalescences noted above, multiple coalescences at a needle tip have been observed before with photographic techniques (e.g. Yoshida et al. 1998). In the experiment of Manasseh et al. (2008), the production of the primary bubble and all following bubbles that coalesced with it were still clearly separated in time from the production of the next primary bubble. Thus the ‘bubbling rate’ f_b was the rate of production of primary bubbles.

In Fig. 2, the time window shows 1 ms bracketing the coalescence event, for the case of $f_b = 3.8 \text{ s}^{-1}$ in which only one coalescence per primary occurs. The time $t = 0$ has been set at the centre time of the frame where coalescence of the primary and secondary bubble occurs. It is clear that the sound pulse is initiated at the very instant of coalescence. It is clear that sound pressure rises during the coalescence event.

The production of sound on coalescence was thought to be a suitable paradigm for comparison with theory. There is no jet formation, which could be quite complex to model, even approximately (e.g. Deane and Czerski 2008). Thus, mechanism (ii) is not occurring at this time. There is no significant relaxation of the bubble shape over the timescale that bubble sound emission commences, making mechanism (iii) less likely. Manasseh et al. (2008) attempted to apply a Laplace-pressure equalisation approach. The variation of acoustic sound amplitude scaled very well with the volume of the small bubble, but the amplitude predicted by an averaged, energetic scaling was an order of magnitude lower than experiment. Therefore, it is of interest to see if a numerical simulation can obtain a better prediction.

NUMERICAL SIMULATIONS OF BUBBLE COALESCENCE

Simulation of bubble coalescence with the axisymmetric level-set method was realised in a computational domain size of $7.68 \times 11.52 \text{ mm}$, described by a uniform 256×384 computational mesh. The bottom and side walls had no-slip boundary conditions and the top of the domain was free slip. The initial radii of the large and small bubbles were 0.8 mm and 0.125 mm respectively, to match the experiment. Bubbles were initially located to match the experiment 0.15 ms prior to coalescence. The bubble density and viscosity were set as 1.2 kg m^{-3} and $1.7 \times 10^{-5} \text{ Pa s}$. The liquid density and viscosity had their physical values of 1000 kg m^{-3} and 0.001 Pa s . The bubbles were assumed to be filled with an ideal gas with $\gamma = 1.4$ and $p_\infty = 0 \text{ Pa}$ and the liquid was assumed to be nearly incompressible with $\gamma = 7.15$ and $p_\infty = 3.05 \times 10^8 \text{ Pa}$. The surface tension coefficient was that of the air-water interface, i.e. 0.074 kg s^{-2} . Other parameters and conditions were chosen to match the conditions of the experiment shown in Figure 1. Monitoring points (P1 and P2) were located on the horizontal line passing through the centre of the large bubble and at $1/3$ and $2/3$ of the domain radius respectively.

The predicted shapes of the bubbles at different times before and after the coalescence are shown in Figure 3. In Figure 4, the experimental observations are shown for the same times. It can be seen that there is a very good agreement in the interfacial kinematics of the coalescence event. In the experiment, the secondary was still attached to the air supply on coalescence, hence re-attaching the primary temporarily. The only significant qualitative differences might be attributed to the fact that in the simulation there was no air supply feeding the secondary bubble immediately after a coalescence.

The numerically simulated frequency of pressure oscillation was 4000 Hz, which agrees well with the natural oscillation frequency of the larger bubble predicted by (2), which is ap-

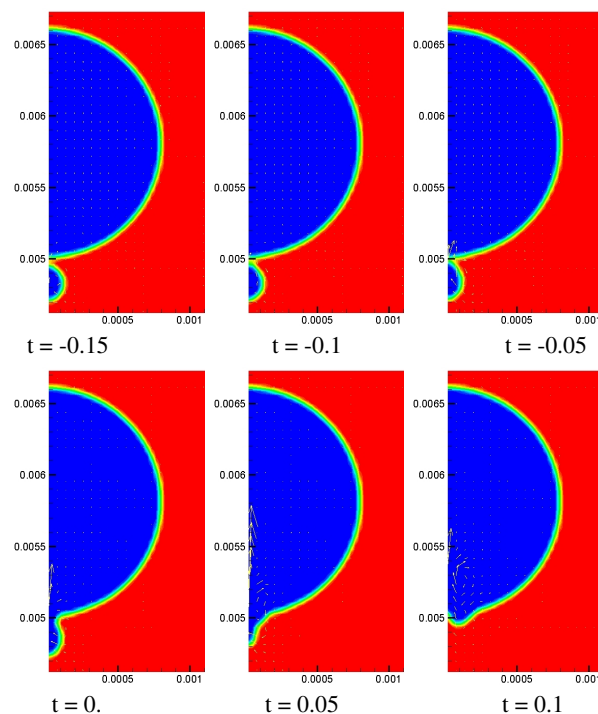


Figure 3: Simulation of the bubble coalescence event of Fig. 1 by the axisymmetric compressible level-set method. Time in ms.

proximately 4077 Hz. Furthermore, the numerically simulated frequency is within about 5% of the experimentally measured frequency of about 4150 Hz. In contrast, the simulated peak pressure at point P1 is about 13 Pa; the experimental data, transformed to P1 using the experimentally-confirmed inverse relation between pressure and distance (Manasseh et al. 2008), was about 20 Pa.

MULTI-MATERIAL NUMERICAL RESULTS

3D free compressible bubble oscillation

In the Rayleigh-Plesset equation (1), the pressure in the bubble, P_g , is related to the equilibrium bubble volume $V_{eq} = 4/3\pi R_0^3$ by

$$P_g = p_0 \left(\frac{V_0}{V} \right), \quad (10)$$

The problem has previously been solved computationally using various approaches, such as boundary elements Blake et al. (1997), Klaseboer and Khoo (2004), front tracking-based finite-difference/finite-volume (FD/FV) computation Hao and Prosperetti (2004), and level-set/VOF FD/FV computation Sussman (2003); common to the bulk of these approaches is the use of an incompressible flow code that models the gas phase by assuming uniformly-distributed vapor pressure, i.e. no gas-sided flow solution.

For the present test, the simulation setup used densities $\rho_G = 1$ and $\rho_L = 1000$ and viscosities $\mu_G = \mu_L = 0$. The small-amplitude volume oscillations for validity of the Rayleigh-Plesset solution involve constant curvature; for flow solver testing, we can ignore surface tension by setting $\sigma = 0$, such that $P_0 = P_\infty$. A bubble of equilibrium bubble radius $R_{eq} = 170 \mu\text{m}$ was initially overexpanded to $R(0) = 171.7 \mu\text{m}$, for a 3% change in mean gas density within the bubble over the oscillation. Based on $\gamma = 1.4$, $p_\infty = 101325 \text{ Pa}$ and polytropic compression, the initial pressure inside the bubble was set to $p_{G0} = 97177.8 \text{ Pa}$. One octant of the sphere was simulated using symmetry boundary conditions at $x = 0$, $y = 0$ and $z = 0$ in conjunction with pressure boundary conditions at $x = X$, $y = Y$ and $z = Z$. Mesh sizes of $76 \times 76 \times 76$ and $112 \times 112 \times 112$ were

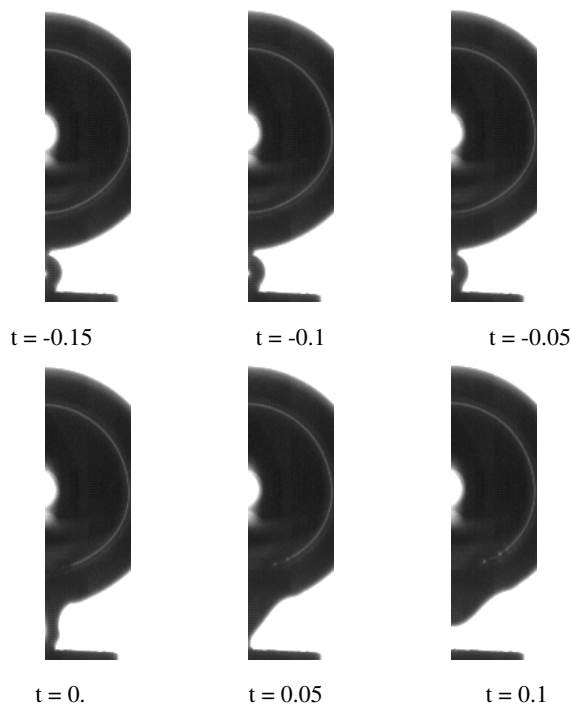


Figure 4: Experimental data for the same times as Fig. 3.

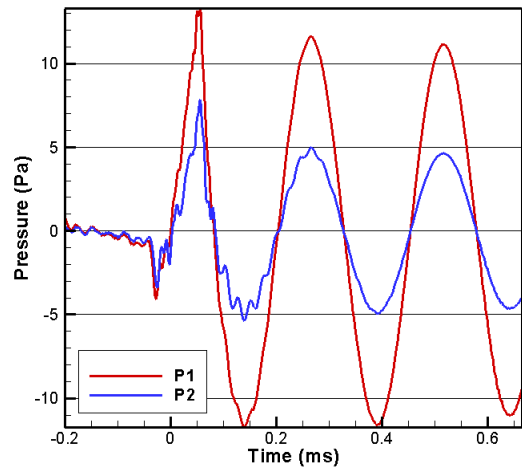


Figure 5: Pressure variation following the bubble coalescence event, simulated by the axisymmetric compressible level-set method.

used to keep the computations feasible with the available resources. Uniform spacings ($\delta x = 6.1111 \mu\text{m}$ in the $76 \times 76 \times 76$ case and $\delta x = 3.4375 \mu\text{m}$ in the $112 \times 112 \times 112$ case) encompassed the entire bubble and immediate surrounds. Mesh coarsening away from the bubble towards the outer boundaries was used to minimize boundary effects and ensure free oscillation; the domain size spanned by the mesh was no smaller than $32R \times 32R \times 32R$.

Figure 6 shows the volume of the bubble compared to the Rayleigh-Plesset solution. The simulated solution captures the periodic contraction and expansion realistically, with good quantitative correspondence achieved using meshes with $> 10^6$ mesh cells. Richardson extrapolation of the $nT/16$ predictions by the simulated solutions at the two different mesh resolutions show close correspondence with the Rayleigh-Plesset solution. The result shows the feasibility of capturing the short time-scale first-order flow induced by volumetrically oscillating bubbles on moderately-sized meshes. The continued approach of the results to the grid-independent result even on the $112 \times 112 \times 112$ mesh motivates continued research towards achieving grid-independence using smaller meshes, through numeric improvements such as sharper discontinuity capturing to better resolve the extrema in the oscillation.

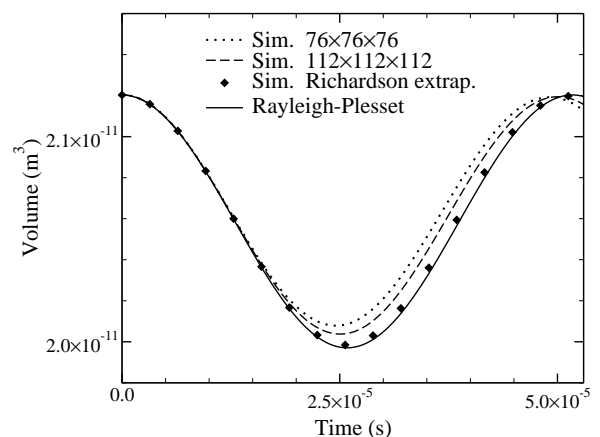


Figure 6: Timeseries of the bubble volume calculated by the compressible multi-material simulation.

3D forced compressible bubble oscillation

To validate the 3D VOF flow solver in cases of both high frequencies and nonlinear dynamics, it was applied to the forced system of Manasseh and Ooi (2005). In the problem, a sphere of gas of radius R_0 at equilibrium pressure P_0 is initialized at the centre of an otherwise liquid flow domain of infinite extent. An oscillating pressure field

$$P_A = \alpha \sin(2\pi f_{ext} t) \quad (11)$$

is applied, where α is the amplitude and f_{ext} is the frequency of the external pressure forcing. Theoretical solutions to the time history of the droplet size for single- and multiple-bubble systems have been generated by Manasseh and Ooi (2005), through solution to an ODE describing the oscillation in radius about the equilibrium initial condition:

$$\left(1 + (N_{bub} - 1) \frac{R_0}{D}\right) \ddot{\varepsilon} \quad (12)$$

$$+ \left(\frac{4\mu}{\rho R_0^3}\right) \dot{\varepsilon} \quad (13)$$

$$+ \left(\frac{3\kappa}{\rho R_0^2} (P_0 + P_v) + (3\kappa - 1) \frac{2\sigma}{\rho R_0^3}\right) \varepsilon = 0, \quad (14)$$

where κ is the ratio of specific heats, N_{bub} is the number of bubbles, P_v is the vapor overpressure, and ρ and μ are the liquid density and viscosity. In the current test, the same input parameters as used in Manasseh and Ooi (2005) were used here – namely, $\rho = 1000$, $\mu = 0.001$, $\kappa = 1.33$, $P_v = 2330$, $P_0 = 100000$ (all in SI MKS units). The current test used a non-uniform $96 \times 96 \times 96$ mesh to simulate an octant of the oscillating bubble, with the bubble resolved using mesh cells of width 6.25×10^{-7} m and aggressive coarsening used away from the bubble to minimize domain truncation effects.

Figure 7 shows the time history generated by the 3D simulation. The capturing of the main harmonic and subharmonics by the simulation is impressive, albeit expensive; to resolve the troughs of the oscillation requires use of $CFL = 0.0001$, with relaxing of this CFL away from the flow reversal represented by the troughs and peaks in the bubble radius. High accuracy in the extrema of bubble radius is more difficult to capture than the temporal locations of these extrema, but clear and reasonable capturing of the extrema in radius was obtained. As shown for the simulation of conventional Rayleigh-Plesset compressible bubble oscillation, higher spatial and temporal resolution is the first and obvious solution to achieving high-fidelity capturing of the extrema in bubble radius in direct numerical simulation using multi-material simulation codes.

Wall effect

Theoretical approaches to generating solutions for bubble oscillation have advanced significantly in their ability to predict compressible bubble oscillation in the presence of walls and in multi-bubble systems, with the review of Manasseh and Ooi (2009) showing quite good capturing of experimentally-measured resonance and natural frequencies by the ODE-based theoretical models. One issue noted in the review is the discrepancy between alternative theories for the prediction of natural frequency of bubble oscillation in the vicinity of walls. Using the self-consistent mirror frequency theory, the natural frequency is

$$\omega = 0.816\omega_0, \quad (15)$$

where ω_0 is the natural frequency in the absence of walls. In contrast, the multiple-scattering mirror frequency theory, the natural frequency is

$$\omega = 0.833\omega_0. \quad (16)$$

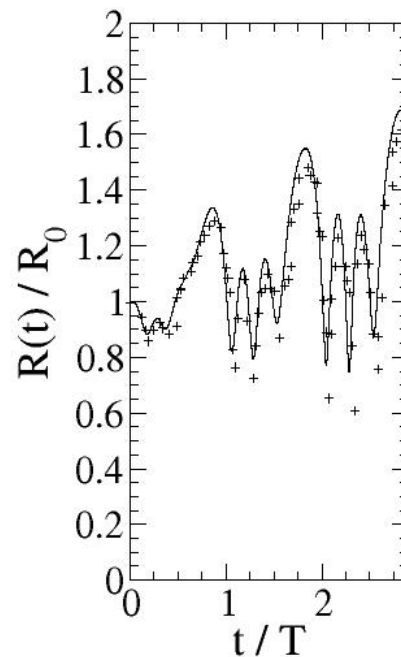


Figure 7: Forced bubble response calculated by the compressible multi-material simulation (continuous line), compared with the nonlinear coupled-oscillator ODE model of Manasseh and Ooi (2005) (+ symbols).

To examine and further validate the 3D VOF multi-material flow solver for this situation, it was used to simulate compressible bubble oscillation at varying distances from a rigid wall. The first at-wall investigation performed as part of this work used an initially overexpanded bubble to drive the oscillation, with an equilibrium radius of $R_0 = 1.7 \times 10^{-4}$ m and initial overexpanded radius $R_{init} = 1.717 \times 10^{-4}$ m representing the distance from the bubble center to the wall. For this case, an $88 \times 88 \times 88$ mesh was used for a quadrant-based simulation, with the bubble resolved by mesh spacing $\delta x = 4.583 \times 10^{-6}$ m and aggressive coarsening in the open directions. An $88 \times 88 \times 176$ was used for the reference no-wall simulation, representing a mirroring of the mesh used in the at-wall simulation.

The simulation of the essentially-at-wall spherical compressible bubble oscillation yielded the reduced frequency $\omega = 0.841\omega_0$. The actual ratio $R_0/s = 0.495$ in the simulation, compared to the $R_0/s = 0.5$ value used to derive equation 15, modifies the multiplier for the self-consistent mirror frequency from 0.816 to 0.818. As such, correcting for the distance $R_{init} - R_0$ separating the wall and the bubble in its equilibrium state, the frequency of oscillation from the simulation is $\omega/\omega_0 = 0.839 \pm 0.01$. The cited error bounds account for both differences between alternatively analyzing bubble pressure and bubble volume signals (indeed seen to be negligible), and sampling error over multiple bubble periods (the larger source). The simulation therefore supports the conclusion that the multiple-scattering mirror frequency better describes compressible bubble oscillation near a wall than the self-consistent mirror frequency theory. The simulation also supports the conjecture in Manasseh and Ooi (2009) that a single bubble and measurement of its radius over time would more inclined result in equation 16 being adhered to as compared to equation 15.

CONCLUSIONS

The quantitative prediction of the amplitude of sound naturally created by bubbles is a demanding task, owing to the variety of fluid-dynamical mechanisms that may be at work. One proposed mechanism (i) involves Laplace-pressure equalisation occurring on the topological change. A second mechanism (ii) invokes the extreme curvature of the gas-liquid interface at the point when there is a change in interface topology and bubbles commence sound emission. The instantaneously-created, very small radii of curvature drive very large, transient accelerations that in turn cause compression or expansion of the gas in the bubble. Another mechanism (iii) proposes a parametric nonlinear process that demands significant excitation of very specific shape modes.

It is hoped that numerical calculations in concert with careful experiments may lead to a prediction of the magnitude of sound created.

Numerical calculations with an axisymmetric, compressible level-set code, simulating actual laboratory conditions, demonstrate excellent prediction of the interface kinematics, very good prediction of the oscillation frequency (within 5%) but much less satisfactory prediction of the amplitude of sound emission, which are roughly 30–40% less than the experimental values. One possible explanation for the discrepancy is domain size, which in lateral extent is an order of magnitude smaller than the experiment. However, if domain limitations are significant, they should significantly alter the frequency, and they clearly do not. A further explanation for the amplitude under-prediction is insufficient resolution, which might prevent correct reproduction of the physics of mechanism (i). In addition, the imposition of axisymmetry may inhibit some modes required by (iii).

As a prelude to systematically testing the various hypotheses for bubble sound emission by numerical experiment, a three-dimensional, multi-material code was set up. Owing to the three-dimensionality, this code had almost an order of magnitude more grid points than the level-set method. A simple spherical perturbation generated a frequency in excellent agreement with analytic frequency. Using this method, the fundamental oscillation frequency of a bubble near a boundary showed a shift in natural frequency owing to the presence of the image of the bubble on the other side of the boundary. These frequency calculations compare very well with analytic theory and experiment, offering further evidence that the limitations of a finite computational domain are not significant, at least for small perturbations to the interface. Thus, a three-dimensional, if computationally intensive, approach may in the future yield a comprehensive prediction of the amplitude of bubble sound emission.

REFERENCES

W. A. Al-Masry, E. M. Ali, and Y. M. Aqeel. Determination of bubble characteristics in bubble columns using statistical analysis of acoustic sound measurements. *Chem. Eng. Res. Design*, 83(A10):1196–1207, 2005.

D. Bhaga and M. E. Weber. In-line interaction of a pair of bubbles in a viscous liquid. *Chem. Eng. Sci.*, 35:2467–2474, 1980.

J.R. Blake, M.C. Hooton, P.B. Robinson, and R.P. Tong. Collapsing cavities, toroidal bubbles and jet impact. *Philos. Tr. R. Soc. S.-A.*, 355:537–550, 1997.

J. W. R. Boyd and J. Varley. The uses of passive measurement of acoustic emissions from chemical engineering processes. *Chem. Eng. Sci.*, 56:1749–1767, 2001.

A. Bui and R. Manasseh. A CFD study of the bubble defor-

mation during detachment. pages Paper 053 1–6. Fifth International Conference on CFD in the Process Industries, Melbourne, Australia, 13–15 December 2006, 2006.

H. Chanson and R. Manasseh. Air entrainment processes of a circular plunging jet: void-fraction and acoustic measurements. *J. of Fluids Eng.*, 125(5):910–921, 2003.

G. B. Deane and H. Czerski. A mechanism stimulating sound production from air bubbles released from a nozzle. *J. Acoustical Soc. Am. Express Lett.*, 123(6):EL126–EL132, 2008.

L. Ding and D. M. Farmer. Observations of breaking surface wave statistics. *J. Phys. Oceanogr.*, 24:1368–1387, 1994.

K. Ellingsen and F. Risso. On the rise of an ellipsoidal bubble in water: oscillatory paths and liquid-induced velocity. *J. Fluid Mech.*, 440:235–268, 2001.

A. Goharzadeh and I. Mutabazi. Experimental characterization of intermittency regimes in the Couette-Taylor system. *Eur. Phys. J. B*, 19:157–162, 2001.

T. R. Hahn, T. K. Berger, and M. J. Buckingham. Acoustic resonances in the bubble plume formed by a plunging water jet. *Proc. R. Soc. Lond. A*, 459:1751–1782, 2003.

Y. Hao and A. Prosperetti. A numerical method for three-dimensional gas-liquid flow computations. *J. Comput. Phys.*, 196:126–144, 2004.

C.W. Hirt and B.D. Nichols. Volume of fluid (vof) method for the dynamics of free boundaries. *J. Comput. Phys.*, 39:205–226, 1981.

C.W. Hirt and B.D. Nichols. Adding limited compressibility to incompressible hydrocodes. *J. Comput. Phys.*, 34:390–400, 1980.

R. Hsi, M. Tay, D. Bukur, G. B. Tatterson, and G. Morrison. Sound spectra of gas dispersion in an agitated tank. *Chem. Eng. J.*, 31:153–161, 1985.

Y. Y. Hu and B. C. Khoo. An interface interaction method for compressible multifluids. *J. Comput. Phys.*, 198:35–64, 2004.

E. Klaseboer and B.C. Khoo. Boundary integral equations as applied to an oscillating bubble near a fluid-fluid interface. *Comput. Mech.*, 33:129–138, 2004.

T. G. Leighton. *The Acoustic Bubble*. Academic Press, London, 1994.

T. G. Leighton and A. J. Walton. An experimental study of the sound emitted by gas bubbles in a liquid. *Eur. J. Phys.*, 8:98–104, 1987.

T. G. Leighton, K. J. Fagan, and J. E. Field. Acoustic and photographic studies of injected bubbles. *Eur. J. Phys.*, 12:77–85, 1991.

P. Liovic and D. Lakehal. Multi-physics treatment in the vicinity of arbitrarily deformable gas-liquid interfaces. *J. Comput. Phys.*, 222:504–535, 2007a.

P. Liovic and D. Lakehal. Interface-turbulence interactions in large-scale bubbling processes. *Int. J. Heat Fluid Flow*, 28:127–144, 2007b.

P. Liovic and D. Lakehal. A newton-krylov solver for remapping-based volume-of-fluid methods. *SIAM J. Sci. Comput.*, 31:865–889, 2008.

P. Liovic, M. Rudman, J. L. Liow, D. Lakehal, and D. B. Kothe. A 3d unsplit-advection volume tracking algorithm with planarity-preserving interface reconstruction. *Comp. Fluids.*, 35:1011–1032, 2006.

P. Liovic, M. Francois, M. Rudman, and R. Manasseh. *J. Comput. Phys.*, , in review., 2009.

M. R. Loewen and W. K. Melville. Microwave backscatter and acoustic radiation from breaking waves. *J. Fluid Mech.*, 224:601–623, 1991.

M. S. Longuet-Higgins. Monopole emission of sound by asymmetric bubble oscillations. part 1. normal modes. *J. Fluid Mech.*, 201:525–541, 1989.

M. S. Longuet-Higgins. An analytic model of sound production

- by raindrops. *J. Fluid Mech.*, 214:395–410, 1990.
- M. S. Longuet-Higgins, B. R. Kerman, and K. Lunde. The release of air bubbles from an underwater nozzle. *J. Fluid Mech.*, 230:365–390, 1991.
- R. Manasseh. Bubble-pairing phenomena in sparging from vertical-axis nozzles. volume 5, pages 27–32. 24th Australian & NZ Chemical Engineering Conference, Sydney, 30 Sep - 2 Oct, 1996.
- R. Manasseh and A. Ooi. Coupled nonlinear oscillations of microbubbles. *ANZIAM J.*, 46:C102–C116, 2005.
- R. Manasseh and A. Ooi. Frequencies of acoustically interacting bubbles. *Bubble Science, Engineering and Technology*, 1(1-2):58–74, 2009.
- R. Manasseh, S. Yoshida, and M. Rudman. Bubble formation processes and bubble acoustic signals. Third International Conference on Multiphase Flow, Lyon, France, 8-12 June, 1998.
- R. Manasseh, A. Bui, J. Sanderkot, and A. Ooi. Sound emission processes on bubble detachment. 14th Australasian Fluid Mechanics Conference, Adelaide University, Adelaide, Australia, 10-14 December 2001, 2001a.
- R. Manasseh, R. F. LaFontaine, J. Davy, I. C. Shepherd, and Y. Zhu. Passive acoustic bubble sizing in sparged systems. *Exp. Fluids*, 30(6):672–682, 2001b.
- R. Manasseh, A. Nikolovska, A. Ooi, and S. Yoshida. Anisotropy in the sound field generated by a bubble chain. *J. Sound Vibration*, 278 (4-5):807–823, 2004.
- R. Manasseh, A. Babanin, C. Forbes, K. Rickards, I. Bobevski, and A. Ooi. Passive acoustic determination of wave-breaking events and their severity across the spectrum. *J. Atmos. Ocean Tech.*, 23(4):599–618, 2006.
- R. Manasseh, G. Riboux, and F. Risso. Sound generation on bubble coalescence following detachment. *International Journal of Multiphase Flows*, 34:938–949, 2008.
- W. K. Melville, M.R. Loewen, F.C. Felizardo, A.T Jessup, and M.J. Buckingham. Acoustic and microwave signatures of breaking waves. *Nature*, 336:54–56, 1988.
- M. Minnaert. On musical air bubbles and the sound of running water. *Phil. Mag.*, 16:235–248, 1933.
- N. De Nevers and J.-L. Wu. Bubble coalescence in viscous fluids. *Am. Inst. Chem. Eng. J.*, 17:182–186, 1971.
- H. Oğuz and A. Prosperetti. Numerical calculation of the underwater noise of rain. *J. Fluid Mech.*, 228:417–442, 1993.
- S. Osher and J.A. Sethian. Fronts propagating with curvature-dependent speed: algorithms based on hamilton-jacobi formulations. *J. Comp. Phys.*, 79:12–49, 1988.
- M.S Plesset and A. Prosperetti. Bubble dynamics and cavitation. *Ann. Rev. Fluid Mech.*, 9:145–185, 1977.
- A. Prosperetti and H. Oğuz. The impact of drops on liquid surfaces and the underwater noise of rain. *Ann. Rev. Fluid Mech.*, 25:577–602, 1993.
- H. C. Pumphrey and L. A. Crum. Free oscillations of near-surface bubbles as a source of the underwater noise of rain. *J. Acous. Soc. Am.*, 87:142–148, 1990.
- H. C. Pumphrey and P. A. Elmore. The entrainment of bubbles by drop impacts. *J. Fluid Mech.*, 220:539–567, 1990.
- Rayleigh. On the pressure developed in a liquid during the collapse of a spherical cavity. *Phil. Mag.*, 34:94–98, 1917.
- M. Rudman. A volume-tracking method for incompressible multi-fluid flows with large density variations. *Int. J. Numer. Methods Fluids*, 28:357–378, 1998.
- C. W. Stewart. Bubble interaction in low-viscosity liquids. *Int. J. Multiphase Flow*, 21(6):1037–1046, 1995.
- M. Strasberg. Gas bubbles as sources of sound in liquid. *J. Acoustical Soc. of America*, 28(1):20–26, 1956.
- M. Strasberg. The pulsation frequency of nonspherical gas bubbles in liquid. *J. Acoustical Soc. of America*, 25(3):536–537, 1953.
- M. Sussman. A second order coupled level set and volume-of-fluid method for computing growth and collapse of vapor bubbles. *J. Comput. Phys.*, 187:110–136, 2003.
- S.Y. Yoon and T. Yabe. The unified simulation for incompressible and compressible flow by the predictor-corrector scheme based on the cip method. *Computer Phys. Communications*, 119:149–158, 1999.
- S. Yoshida, R. Manasseh, and N. Kajio. The structure of bubble trajectories under continuous sparging conditions. volume 426, pages 1–8, Lyon, France, June, 1998. 3rd International Conference on Multiphase Flow.